Monthly Notices
of the
ROYAL ASTRONOMICAL SOCIETY

MNRAS **482,** 698–714 (2019)
Advance Access publication 2018 October 2

doi:10.1093/mnras/sty2653

The Ophiuchus DIsc Survey Employing ALMA (ODISEA) – I: project description and continuum images at 28 au resolution

Lucas A. Cieza,[1,2]★ Dary Ruíz-Rodríguez,[3]★ Antonio Hales,[4,5] Simon Casassus,[2,6] Sebastian Pérez,[2,6] Camilo Gonzalez-Ruilova,[2,6] Hector Cánovas,[7] Jonathan P. Williams,[8] Alice Zurlo,[1,2] Megan Ansdell,[9] Henning Avenhaus,[10] Amelia Bayo,[11,12] Gesa H.-M. Bertrang,[2,6,13] Valentin Christiaens,[2,6] William Dent,[4] Gabriel Ferrero,[14] Roberto Gamen,[14] Johan Olofsson,[11,12] Santiago Orcajo,[14] Karla Peña Ramírez,[15] David Principe,[16] Matthias R. Schreiber[11,12] and Gerrit van der Plas[17]

Affiliations are listed at the end of the paper

Accepted 2018 September 20. Received 2018 September 15; in original form 2018 August 10

ABSTRACT

We introduce the Ophiuchus DIsc Survey Employing ALMA (ODISEA), a project aiming to study the entire population of *Spitzer*-selected protoplanetary discs in the Ophiuchus Molecular Cloud (∼300 objects) from both millimetre continuum and CO isotopologues data. Here we present 1.3 mm/230 GHz continuum images of 147 targets at 0.2 arcsec (28 au) resolution and a typical rms of 0.15 mJy. We detect a total of 133 discs, including the individual components of 11 binary systems and 1 triple system. 60 of these discs are spatially resolved. We find clear substructures (inner cavities, rings, gaps, and/or spiral arms) in eight of the sources and hints of such structures in another four discs. We construct the disc luminosity function for our targets and perform preliminary comparisons to other regions. A simple conversion between flux and dust mass (adopting standard assumptions) indicates that all discs detected at 1.3 mm are massive enough to form one or more rocky planets. In contrast, only ∼50 discs (∼1/3 of the sample) have enough mass in the form of dust to form the canonical 10 $M_\oplus$ core needed to trigger runaway gas accretion and the formation of gas giant planets, although the total mass of solids already incorporated into bodies larger than cm scales is mostly unconstrained. The distribution in continuum disc sizes in our sample is heavily weighted towards compact discs: most detected discs have radii < 15 au, while only 23 discs (∼15 per cent of the targets) have radii > 30 au.

Key words: protoplanetary discs – circumstellar matter – stars: pre-main-sequence – submillimetre: planetary systems.

1 INTRODUCTION

The diversity and high incidence of extrasolar planets in the field (Cassan et al. 2012; Howard 2013; Burke et al. 2015; Shvartzvald et al. 2016) demonstrate that planet formation processes are efficient and imply that most of the circumstellar discs seen in nearby molecular clouds should form planetary systems. Studying the structure and evolution of complete populations of protoplanetary discs in these clouds is thus important to place constraints on the conditions, time-scales, and mechanisms associated with planet formation. Early-science observations of individual protoplanetary discs with the Atacama Large Millimeter/submillimeter Array (ALMA) have produced transformational results (Casassus et al. 2013; Van Der Marel et al. 2013; ALMA Partnership et al. 2015; Andrews et al. 2016; Cieza et al. 2016; Pérez et al. 2016). However, detailed submillimetre studies tend to target bright sources ($F_{\rm mm} \gtrsim 50$ mJy) and are therefore very biased towards massive discs around relatively massive stars. Also, many imaging studies have focused on bright 'transition objects' (e.g. massive discs with inner holes and gaps tens of au wide). While very important, such objects are *not* representative of the typical planet-forming disc in a molecular cloud; they only represent $\lesssim$10 per cent of the young disc population (Cieza et al. 2012a). The disc population is very

★ E-mail: lucas.cieza@mail.udp.cl (LAC); darpci@rit.edu (DRR)

diverse, which might reflect a wide range of initial conditions (Bate 2018) and evolutionary paths (Cieza et al. 2007; Currie & Kenyon 2009). Transition discs with large cavities could be related to the formation of multiple giant planets (Owen 2016), which are rare according to extrasolar planet studies. On the other hand, planetary systems with low-mass planets are much more common in the Galaxy. In particular, Gaidos et al. (2016) estimate that M-dwarfs, the most common type of star in the Milky Way, host an average of 2.2 ± 0.3 planets with radii of 1–4 $R_\oplus$ and orbital periods less than 180 d. Such planets could in principle form in discs that are only a few au in radius and contain just a few Earth masses of dust.

Previous infrared surveys with *Spitzer*, tracing mostly optically thick emission, have shown that the *presence* of a disc is a strong function of stellar age and that protoplanetary discs have a mean lifetime of ∼3 Myr (Williams & Cieza 2011). ALMA's unprecedented sensitivity provides, for the first time, the opportunity to study complete samples of discs at sub-arcsecond resolution in the (sub)millimetre regime, where discs become optically thin and resolved images trace the spatial distribution of mass. ALMA has already surveyed many of the nearby ($\lesssim$250 pc) disc populations: Ansdell et al. (2016, Ansdell et al. 2018) observed ∼90 discs in Lupus, Barenfeld et al. (2016) studied 106 objects in the Upper Scorpius OB Association, and Pascucci et al. (2016) investigated 93 discs in the Chamaeleon I star-forming region. Similarly, Ansdell et al. (2017) studied 92 objects in σ Ori, Cox et al. (2017) observed 49 systems in Ophiuchus, and Ruíz-Rodríguez et al. (2018) studied 136 discs in the IC 348 cluster. In general, these surveys observe gas tracers (^{12}CO, ^{13}CO, and/or C^{18}O) and dust continuum. Since the dust continuum is easier to detect and study, total disc masses are typically derived assuming a gas-to-dust mass ratio of 100. Under this assumption, surveys usually find a very wide range of discs masses (<1 to ∼100 M_{JUP}) and a strong dependence of disc mass on stellar mass. A clear overall decrease on disc mass with stellar age is also seen; however, some discs remain undetected at mm wavelengths at very young ages ($\lesssim$1 Myr) while a few massive discs are still seen in older regions ($\gtrsim$5 Myr). Studies attempting to derive gas masses from CO isotopologues often find gas-to-dust mass ratios significantly lower than 100, but it remains to be established whether these results reflect the depletion of total gas mass or just volatile carbon (Ansdell et al. 2016; Miotello et al. 2017).

As part of the Ophiuchus DIsc Survey Employing ALMA (ODISEA) project, here we present Band-6 (230 GHz/1.3 mm) continuum observations of 147 discs in the Ophiuchus Molecular Cloud at a spatial resolution of 0.2 arcsec (28 au). This is the largest (sub)millimetre disc study at this physical resolution to date and represents 50 per cent of the full ODISEA sample (see Section 2.1). Together with the Taurus Molecular cloud, Ophiuchus has been one of the best-studied regions in the (sub)millimetre regime in the pre-ALMA era and it has played a central role in our understanding of protoplanetary disc populations. Andrews & Williams (2007) presented single-dish submillimetre observations for 48 Ophiuchus sources (resolution = 14 arcsec and rms ∼5 mJy at 850 μm). They also collected 1.3 mm measurements for 99 additional targets from the literature (rms ∼10 mJy), for a total sample of 147 objects (the same number as in this paper, but not necessarily all the same sources), resulting in 64 detected objects with estimated disc masses between 1 and 200 M_{JUP}. They estimate that the typical disc in their sample has 1 per cent of the stellar mass. Cieza et al. (2010) presented (sub)millimetre photometry for 26 Ophiuchus 'transition discs', broadly defined there as objects with reduced levels of infrared excess with respect to the median found in T Tauri stars[1] with a similar disc mass sensitivity of ∼1 M_{JUP}. They found that accreting transition objects tend to have discs that are bright in the (sub)millimetre, while non-accreting transition objects tend to have much fainter discs that are usually undetected at (sub)millimetre wavelengths. Andrews et al. (2009, 2010) used the Submillimeter Array to image 17 of the brightest Ophiuchus discs (75 > mJy at 850 μm) at a 0.3 arcsec resolution and found that 4 of them had resolved inner cavities. More recently, Cox et al. (2017) used ALMA to observe 49 Ophiuchus systems at 870 μm with a resolution of 0.2 arcsec in dust continuum only, making it the largest survey of resolved protoplanetary discs in Ophiuchus before ODISEA. They find that binary systems tend to have smaller and lower mass discs and identified at least four objects with gaps and/or inner cavities in their discs.

The ODISEA project aims to produce a complete demographic study of the discs in Ophiuchus to investigate disc evolution and the planet formation potential of the entire cloud. This is the first of a series of papers that will also include (1) a study of disc properties as a function of the mass and age of the host stars (Ruíz-Rodríguez et al. in preparation), (2) an investigation of the effects of (sub)stellar companions on disc properties (Zurlo et al. in preparation), (3) radiative transfer modelling of resolved sources (Pérez et al. in preparation), and (4) a study of gas content in the discs based on ^{12}CO, ^{13}CO, and/or C^{18}O observations (Williams et al. in preparation). In Section 2, we discuss the sample selection for the ODISEA project and our ALMA Cycle-4 observations. In Section 3, we present our dust continuum images. We measure dust continuum fluxes and disc sizes for all resolved sources and provide deprojected radial profiles to search for discs showing substructures (inner cavities and gaps). In Section 4, we compare our results to those of previous surveys and discuss their implications for disc evolution and planet formation. A summary of our main results and conclusions is presented in Section 5.

2 SAMPLE SELECTION AND ALMA OBSERVATIONS

2.1 Sample selection

At a distance of 140 ± 10 pc (Ortiz-León et al. 2017; Canovas et al. in preparation), Ophiuchus is the closest star-forming region with at least ∼300 discs. The ODISEA sample is the full catalogue of 297 young stellar objects (YSOs) in Ophiuchus from the *'Cores to Discs' Spitzer* Legacy Programme (Evans et al. 2009b). YSOs are usually divided into different classes based on their spectral slopes,

$$\alpha_{IR} = \frac{\log(\lambda_1 F_{\lambda_1}) - \log(\lambda_0 F_{\lambda_0})}{\log(\lambda_1) - \log(\lambda_0)}, \quad (1)$$

where F_λ is the flux density at λ_1 and λ_0, corresponding to ∼2 and ∼20 μm, respectively (Greene et al. 1994; Chen et al. 1995). Class I sources have $\alpha_{IR} > 0.3$ and are typically associated with very young objects deeply embedded in their envelopes. Flat spectrum sources have $0.3 > \alpha_{IR} > -0.3$ and are less embedded systems, but presumably still retain some detectable emission from the envelope. Class II objects have $-0.3 > \alpha_{IR} > -1.6$ and are sources where the infrared excess arises almost exclusively from an optically thick

[1]Transition discs have been defined in several different ways in the literature, see for example the *diskionary* by Evans et al. 2009a; https://arxiv.org/pdf/0901.1691.pdf.

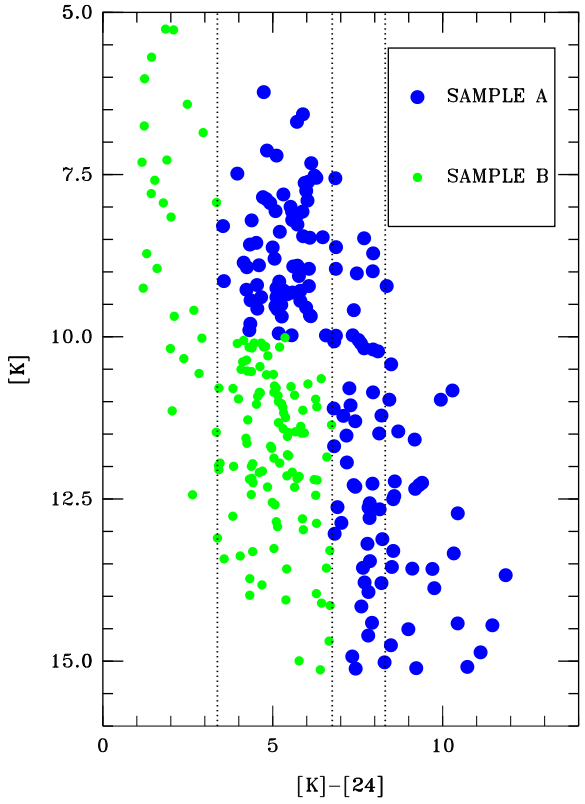

Figure 1. The [*K*] versus [*K*]–[24] colour–magnitude diagram of the full sample of *Spitzer* Young Stellar Object Candidates in Ophiuchus identified by the *Cores to Discs* Legacy Programme. The vertical lines are the approximate boundaries between Class III, Class II, Flat Spectrum, and Class I objects (left to right). The *Spitzer* objects were divided into two ODISEA samples. Sample 'A', presented in this paper, contains 147 objects, which are Class I and Flat Spectrum sources together with Class II objects brighter than 10 mag in *K* band.

circumstellar disc. Finally, Class III sources have $\alpha_{\rm IR} < -1.6$ and are more evolved systems with little or no disc emission up to 20 μm.

Using these classes as a guide, the full ODISEA sample is divided into two subsamples, as shown in Fig. 1. Sample A contains all Class I and Flat Spectrum sources, specifically objects with [*K*]–[24] > 6.75 mag, and Class II sources with $K > 10$ mag. Sample B contains all Class III discs (they all have weak but significant, $>5\sigma$, IR excesses) and Class II sources fainter than 10 mag in *K* band. The boundary in *K* band was chosen so that the two subsamples have $\lesssim$150 targets, which allows us to fit each subsample in a single Science Goal in the ALMA Observing Tool and maximizes the efficiency of the observations. Both samples, A and B, were observed in ALMA Cycle-4, but the observations for Sample B were not successful due to a scripting problem at the observatory that prevented the proper cycling between targets and phase calibrators. As a result, only a few targets from Sample B were observed and the observations did not pass the quality assessment performed by the observatory. Therefore, in this paper we focus on the 147 sources from Sample A, which are listed in Table 1. Table 2 shows the 2MASS and *Spitzer* photometry from these 147 objects, taken from the NASA/IPAC Infrared Science Archive.[2] The ODISEA project was approved again for ALMA Cycle-5, and at the time of this writing, the observations for Sample B have started, but have not yet been completed. We emphasize that Samples A and B are not equivalent. Objects in Sample B are expected to be, on average, significantly fainter at millimetre wavelengths since (1) Class II objects that are fainter in *K* band tend to have lower (sub)stellar masses and disc masses correlate with the mass of the central object (Andrews et al. 2013) and (2) Class III discs tend to have very low dust masses (< 0.3 M$_\oplus$; Hardy et al. 2015; Cieza et al. 2013).

2.2 The completeness of the *Spitzer* disc census

The spatial distributions of both Samples A and B are shown in Fig. 2 overlaid in the *Spitzer* map of the 'Cores to Discs' Legacy Project (Evans et al. 2009b). The map covers a region with an area of 6.6 deg^2 in the sky. Within this region, the *Spitzer* catalogue has the following 90 per cent completeness limits: 0.018, 0.020, 0.066, 0.100, and 0.700 mJy at 3.6, 4.5, 5.8, 8.0, and 24 μm. Since less than a Moon mass of warm dust ($T \sim$ 100–300 K) is needed to produce an optically thick excess emission above the stellar photosphere in the mid-infrared (∼8–24 μm), this *Spitzer* catalogue represents an essentially complete IR census of the optically thick disc population in the stellar mass regime and extends well into the substellar members (Allers et al. 2006). The extinction at 24 and 8 μm is only 2.5 and 5 per cent of the visual extinction, respectively. Therefore, extinction does not affect significantly the completeness of the survey. In fact, highly embedded targets tend to be very young Class I objects, where the accretion luminosity increases the mass sensitivity of the IR observations (Evans et al. 2009b). Dunham et al. (2008) estimate the sensitivity of the 'Cores to Discs' survey to be 4×10^{-4} L$_\odot$ for embedded protostars at 140 pc, also well below the stellar/substellar boundary.

For Class III sources with small IR excesses above the stellar photosphere, the sensitivity of the *Spitzer* survey is mostly given by the photospheric fluxes at 24 μm of stars of different masses and ages. Wahhaj et al. (2010) find that the 'Cores to Discs' survey can reach the stellar photospheres of 0.3–0.5 M$_\odot$ pre-main-sequence stars at 140 pc for ages in the 1–3 Myr range. Such discs typically have low luminosities ($L_{\rm disc}/L_{\rm star} \lesssim 10^{-3}$) and are optically thin at mid-IR wavelengths. Hardy et al. (2015) observed 24 *Spitzer*-selected Class III discs with ALMA using a sensitivity similar to that of ODISEA. They detected only four targets in the continuum and none of them in CO, suggesting that these Class III objects are in a very advanced stage of disc dispersal or already in the debris disc phase. Therefore, while some Class IIII discs around very low mass stars ($\lesssim$0.3–0.5 M$_\odot$) might be missing in the *Spitzer* catalogues, those objects are unlikely to be detected by a snapshot survey like ODISEA. In principle, *Spizer* observations could miss discs with no mid-IR excesses (λ ∼ 8–24 μm), but significant far-IR (λ ∼ 70–250 μm) emission. However, far-IR surveys with *Herschel* show that those systems are very rare and are consistent with cold debris discs or background galaxies (Cieza et. 2013; Gáspár & Rieke 2014; Rebollido et al. 2015). In summary, the *Spitzer* disc census in the area mapped by the 'Cores to Discs' project can be considered to be complete in the stellar mass regime for Class I and Class II sources, but might become incomplete for Class III sources, especially around very low mass stars ($\lesssim$0.3–0.5 M$_\odot$).

[2] http://irsa.ipac.caltech.edu/Missions/spitzer.html

Table 1. ODISEA Cycle-4 SAMPLE.

ID	C2D ID	RA (J2000.0)	Dec. (J2000.0)	RA (deg)	Dec. (deg)	SpT	Ref1	Separation (arcsec)	Ref2
1	SSTc2d J162131.9-230140	16:21:31.920	−23:01:40.25	245.382 996	−23.027 847	–	–	–	–
2	SSTc2d J162138.7-225328	16:21:38.722	−22:53:28.26	245.411 346	−22.891 182	–	–	–	–
3	SSTc2d J162145.1-234232	16:21:45.127	−23:42:31.63	245.438 034	−23.708 786	–	–	–	–
4	SSTc2d J162148.5-234027	16:21:48.473	−23:40:27.26	245.451 965	−23.674 240	–	–	–	–
5	SSTc2d J162218.5-232148	16:22:18.521	−23:21:48.12	245.577 164	−23.363 367	K5	1	0.02	1
6	SSTc2d J162221.0-230402	16:22:20.990	−23:04:02.35	245.587 463	−23.067 320	–	–		–
7	SSTc2d J162225.0-232955	16:22:24.950	−23:29:54.91	245.603 958	−23.498 587	–	–	–	–
8	SSTc2d J162245.4-243124	16:22:45.389	−24:31:23.82	245.689 117	−24.523 283	M3	1	0.54	2
9	SSTc2d J162305.4-230257	16:23:05.431	−23:02:56.73	245.772 629	−23.049 091	–	–	–	–
10	SSTc2d J162306.9-225737	16:23:06.859	−22:57:36.61	245.778 580	−22.960 171	–	–	–	–

Note.
Comments: Only the first 10 lines are shown. The full table is available online. References for spectral types are as follows: 1 = Cieza et al. (2010); 2 = Erickson et al. (2011); 3 = Wilking et al. (2005); 4 = Manara et al. (2015); 5 = McClure et al. (2010); 6 = Cieza et al. (2007); 7 = Luhman & Rieke (1999). Reference for multiplicity are as follows: 1 = Ruíz-Rodríguez et al. (2016); 2 = Cieza et al. (2010); 3 = Ratzka, Köhler & Leinert (2005); 4 = Loinard et al. (2008); 5 = This work; 6 = Kohn et al. (2016).

Table 2. Photometry from the *Spitzer* Cores to Discs Catalogue.

ID	J	eJ	H	eH	K	eK	$F_{3.6}$	$eF_{3.6}$	$F_{4.5}$	$eF_{4.5}$	$F_{5.8}$	$eF_{5.8}$	$F_{8.0}$	$eF_{8.0}$	F_{24}	eF_{24}	F_{70}	eF_{70}
									(mJy)									
1	36.10	0.86	80.60	1.93	103.00	2.00	101.00	5.03	85.00	4.23	73.90	3.51	79.40	3.86	119.0	11.0	175	25
2	0.25	0.05	0.46	0.07	0.60	0.09	0.81	0.04	0.97	0.05	1.46	0.08	5.68	0.27	31.7	2.9	–	–
3	0.50	0.05	1.33	0.08	2.47	0.12	5.50	0.28	9.11	0.45	7.26	0.36	14.30	0.70	201.0	18.6	704	87
4	5.82	0.15	11.80	0.29	14.10	0.27	12.40	0.60	12.00	0.57	10.80	0.52	15.20	0.73	79.9	7.3	–	–
5	249.00	5.51	376.00	14.50	380.00	10.20	383.00	30.30	289.00	18.80	247.00	13.60	266.00	17.3	808.0	74.90	875	98
6	2.19	0.08	2.90	0.10	2.48	0.10	1.61	0.08	1.60	0.08	1.78	0.10	7.72	0.38	117.0	10.8	–	–
7	57.20	1.26	96.20	2.04	98.50	1.91	118.00	5.99	117.00	5.84	102.00	4.87	107.00	5.35	120.0	11.1	–	–
8	113.00	2.49	172.00	4.11	158.00	3.64	92.10	4.58	61.50	3.04	44.70	2.14	51.30	2.47	345.0	32.0	–	–
9	1.86	0.06	2.93	0.07	3.19	0.11	2.36	0.12	2.66	0.13	3.43	0.18	5.53	0.27	89.8	8.3	–	–
10	0.33	0.04	0.64	0.07	1.45	0.09	3.94	0.20	5.96	0.29	8.20	0.40	10.10	0.48	17.2	1.6	–	–

Note.
Comments: Only the first 10 lines are shown. The full table is available online.

2.3 Observations and data reduction

All of our 147 targets in Sample A were observed under the Cycle-4 ALMA programme 2016.1.00545.S on a single scheduling block, which was executed 3 times between 2017 July 13 and 14.[3] The nominal array configuration was C40-5, and 42–45 of the 12 m ALMA antennas were used with baselines ranging from 17 to 2647 m. The precipitable water vapour ranged from 1.1 to 1.9 mm during the observations. The objects J1517-2422 and J1733-1304 were observed as flux calibrators, while the quasars J1517-2422 and J1625-2527 were used as bandpass and phase calibration, respectively. The ALMA correlator set-up was the following: three spectral windows were centred at 230.538 000, 220.398 684, and 219.560 358 GHz to cover the ^{12}CO J = 2–1, ^{13}CO J = 2–1, and C^{18}O J = 2–1 transitions, respectively. All three windows had a spectral resolution of 0.08 km s^{-1}. The first spectral window had a bandwidth of 117 MHz, while the other two had 58.6 MHz bandwidths. Two additional spectral windows, centred at 233.00 and 218.00 GHz, had 1.875 GHz bandwidths and were selected for continuum observations, for a total continuum bandwidth of 3.98 GHz.

All data were calibrated using the Common Astronomy Software Applications package (CASA v4.4; McMullin et al. 2007) by the ALMA observatory. The standard calibration included offline water vapour radiometer calibration, system temperature correction, bandpass, phase, and amplitude calibrations.

The observations from all three nights were concatenated and processed together to increase the signal to noise and *uv*-coverage. The flux calibration in the three epochs agreed within < 10 per cent and thus no rescaling of the flux was applied. We used the CLEAN algorithm to image the data adopting Briggs weights and robust parameter equal to zero as a balance between resolution and sensitivity. For the continuum, we obtained a typical rms of ∼0.15 mJy beam^{-1} and a synthesized beam of 0.28 arcsec × 0.19 arcsec. The molecular line data (^{12}CO, ^{13}CO, and C^{18}O) will be discussed in another paper of the series (Williams et al. in preparation).

[3]We note that previous observations of Sample A suffered from the same scripting problem as Sample B and are not included in this paper. The failed observations for Sample A correspond to execution blocks uid://A002/Xc1c1f1/X81bc (2017 July 7) and uid://A002/Xc1e2be/X717 (2017 July 9). The failed observations for Sample B correspond to execution blocks uid://A002/Xbfb22d/X1b7f (2017 April 27) and uid://A002/Xbfb22d/X84ed (2017 April 28).

3 RESULTS

3.1 Continuum images, disc photometry, and sizes

We used the Viewer task within CASA to individually inspect all the images. In the majority of the cases, we found a single 1.3 mm detection within < 1 arcsec of the nominal location of the *Spitzer*

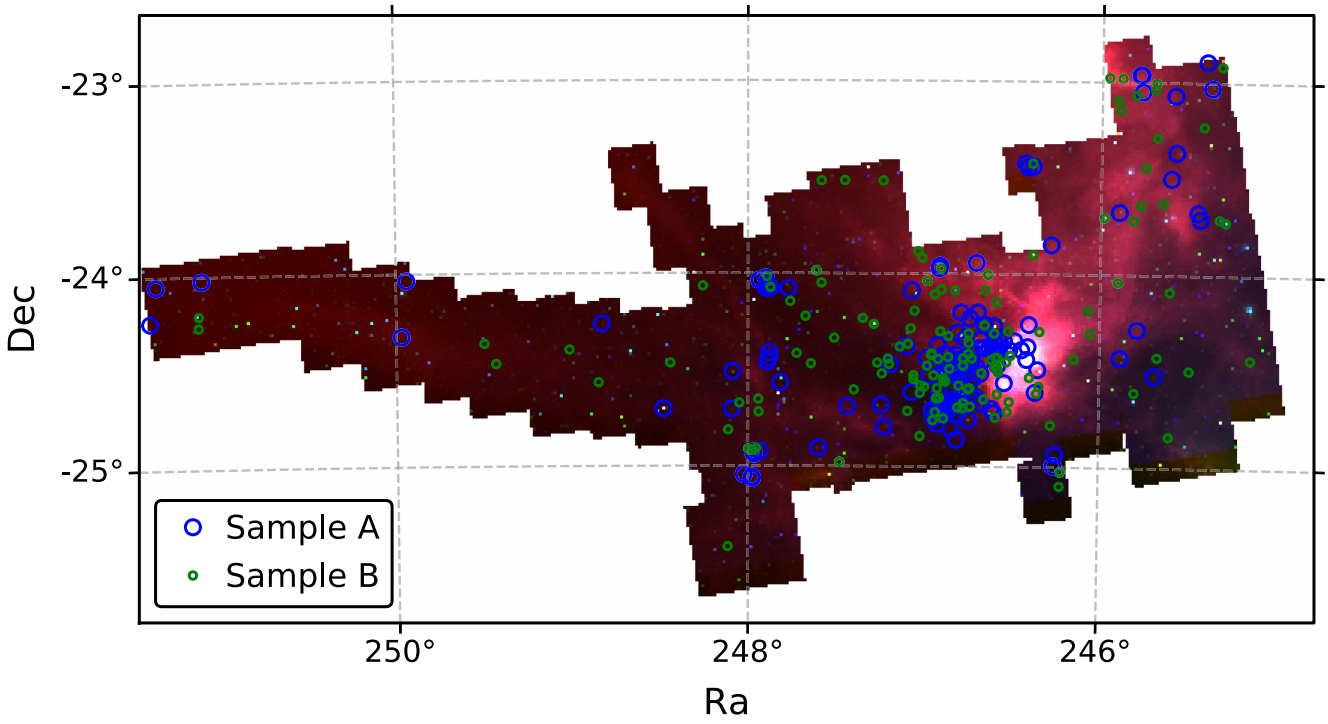

Figure 2. The spatial distribution of the ODISEA targets (both Samples A and B) shown on top of the *Spitzer* map of the Ophiuchus molecular cloud from the 'Cores to Discs' Legacy Project.

source that can be unambiguously identified as the target.[4] We first used the *imstat* task to search for the peak flux value within an aperture of 1 arcsec in radius and calculated an rms from an annulus with inner and outer radii of 1.0 arcsec and 1.2 arcsec, respectively. For *single* objects with peak signal-to-noise ratios (S/N) > 5, we used the *uvmodelfit* task in CASA to derive basic parameters for each source. The full spectral coverage was utilized. We fitted both a point source and Gaussian with all free parameters: the integrated flux density, the full width at half-maximum (FWHM) along the major and minor axis, the position angle (PA), and small offsets ($<$ 1.0 arcsec) in right ascension and declination from the phase centre. We find that for objects with peak S/N $\lesssim 30$, the point source and the Gaussian fits give similar fluxes, but the Gaussian fits produce FWHM and PA values with very large uncertainties ($\gtrsim$50 per cent and $\gtrsim$90 deg, respectively). For objects with high S/N, the Gaussian fit can measure FWHM values (deconvolved from the beam) down to a factor of $\sim$2 of the beam size, but the ability to measure the FWHM and the PA of the disc depends on both the size and the S/N of the source. For sources with sizes (i.e. FWHM values of major axes) comparable to the beam, the Gaussian and point source fit give similar fluxes, although the Gaussian fit tends to give slightly larger fluxes (by $\sim$10 per cent). For more extended sources, the point source fit significantly underestimates the flux.

Ideally, one would use the ratio of the FWHM value to its uncertainty to establish whether a source is spatially resolved. However, the *uvmodelfit* documentation indicates that the size uncertainties are likely to be underestimated by this task. Therefore, we use *ad hoc* criteria to decide whether the source is spatially resolved (i.e. sufficiently different from a point source to justify reporting disc sizes and orientations). In particular, we provide size information only if the source has a peak S/N > 30 and the Gaussian flux is greater than the point source flux plus 3 times the rms of the sky between 1 and 1.2 arcsec of the target. For resolved sources, we report the 1σ uncertainties obtained for each parameter (except for the position), but remind the reader that these uncertainties might be underestimated. Otherwise, we consider the source to be unresolved and only report the flux and its uncertainty. For the few objects with significant substructures (e.g. transition disc objects with cavities, spiral arms, and/or wide gaps, targets # 12, 22A, 51, 41, 62, 127, 141, and 143, see Section 3.4), the Gaussian model does not provide an accurate fit. In these cases, we fit an elliptical disc model to measure their sizes (also within *uvmodelfit*), but we use the 2D fitting tool within the CASA Viewer to measure the flux using a sufficiently large aperture, typically $\sim$3 arcsec in radius.

For multiple sources (doubles and triples), we also measure fluxes and discs sizes (also expressed in terms of the FWHM of the major axes) in the image plane using the 2D fitting tool within CASA. This tool provides size and PA information for spatially resolved objects that have enough S/N. Otherwise, the task indicates that the source is consistent with a point source. For these multiple sources, we use the convergence of the fitting tool as the detection criteria of the sources.

For non-detected targets, we still estimate and report the flux and rms at the expected location of the source using *uvmodelfit* to fit a point source. From all the detections, we find average offsets in RA and Dec. of -0.08 arcsec and -0.56 arcsec, respectively, which we attribute to the proper motions of the targets based on the results of the *Gaia* Data Release 2 (Gaia Collaboration 2018). Canovas et al. (in preparation) found Gaia proper motions of $\mu_\alpha = -6.9 \pm 1.6$ and

[4]The only exception object 62, where a 180 mJy detection is displaced 5 arcsec with respect to the *Spitzer* coordinates. The detection corresponds to the object EM $*$ SR 24S, which is part of a triple system that also contains the SR 24 Nb and SR 24Nc components. We note that the *Spitzer* coordinates correspond to the northern pair, which is only 0.34 mJy at 1.3 mm (Fernández-López et al. 2017).

Table 3. Fluxes and sizes at 1.3 mm from Cycle-4.

ODISEA C4 ID	RA (J2000.0)	Dec. (J2000.0)	$F_{1.3}$ (mJy)	$eF_{1.3}$ (mJy)	Major (mas)	eMajor (mas)	Minor (mas)	eMinor (mas)	PA (deg)	ePA (deg)
ODISEA_C4_001	16:21:31.924	−23:01:40.79	4.60	0.16	–	–	–	–	–	–
ODISEA_C4_002	–	–	0.17	0.20	–	–	–	–	–	–
ODISEA_C4_003	16:21:45.123	−23:42:32.19	40.09	0.23	541.0	3.6	97.2	5.0	174.2	1.0
ODISEA_C4_004	16:21:48.474	−23:40:27.76	3.25	0.31	–	–	–	–	–	–
ODISEA_C4_005	16:22:18.522	−23:21:48.62	29.84	0.24	184.4	4.9	133.2	6.0	108.7	0.3
ODISEA_C4_006	–	–	− 0.19	0.13	–	–	–	–	–	–
ODISEA_C4_007	16:22:24.953	−23:29:55.41	13.57	0.18	–	–	–	–	–	–
ODISEA_C4_008	–	–	− 0.03	0.31	–	–	–	–	–	–
ODISEA_C4_009	16:23:05.418	−23:02:57.49	5.24	0.19	–	–	–	–	–	–
ODISEA_C4_010	–	–	0.73	0.13	–	–	–	–	–	–

Note.
Comments: Only the first 10 lines are shown. The full table is available online. The ODISEA_C4 designation indicates that the data were obtained in ALMA Cycle-4. The next number denotes the corresponding target in Table 1. Sources with no RA and Dec. information have not been detected by our ALMA observations. Sources with position information but no size information have been detected but remain unresolved. The major and minor axis information corresponds to FWHM values.

$\mu_\delta = -25.6 \pm 1.7$ arcsec yr^{-1} for a sample of ∼200 Ophiuchus discs (most, but not necessarily all, are included in our ALMA sample). Since the *Spitzer* catalogues from the 'Cores to Discs' project (Evans et al. 2009b) used to select our targets were tied to 2MASS coordinates (Cutri et al. 2003), there is an ∼18 yr difference between the *Spitzer* coordinates and the ALMA observations. This should translate to a shift in coordinates of ∼0.1 arcsec and ∼0.5 arcsec in RA and Dec., respectively, consistent with the observed offsets. Because the mean displacement is larger than the beam, we apply the observed offsets to the nominal position of the non-detected targets before fitting a point source at the new location.

Given the different methods used to estimate the photometry and the disc sizes, we emphasize that the fluxes should be taken with caution, especially for objects with clear substructures. We also note that all the fluxes are subject to a 10 per cent calibration uncertainty. All the information on disc sizes and fluxes, obtained as described above, is listed in Table 3.

We detect a total of 133 discs in 120 systems. These 133 discs correspond to 108 single discs plus the individual components of 11 binary discs and 1 triple-disc system, leaving 27 targets undetected. Fig. 3 shows the 53 single discs with size information ordered by decreasing integrated flux. Many of the brightest sources are clearly extended, while most of the fainter sources tend to be only partially resolved. Fig. 4 shows the 55 single discs that are detected but are consistent with a point source at the resolution of our observations (∼0.2 arcsec). The vast majority (49/55) of these sources are fainter than ∼10 mJy. Multiple targets (11 binaries and 1 triple system) are highlighted in Fig. 5. In Table 3, we add an 'A' to the source ID to denote the component that is closer to the nominal coordinates from *Spitzer* (i.e. the centre of the ALMA pointing) and a 'B' to denote the other source. In the case of the triple system, the source farthest away from the ALMA pointing is defined as the 'C' component.

3.2 Stacking of non-detections

To estimate the typical flux of the discs that were not detected, we stack the images of the 27 non-detections, calculating the mean of each pixel from the individual images centred at the nominal location of each target. The results are seen in Fig. 6. The stacked image has an rms of 0.04 mJy and shows a 4σ (0.16 mJy) detection shifted −0.5 arcsec in Dec. This offset is very consistent with the mean offset in Dec. found for the detected discs (−0.56 arcsec) and suggests that the detection is real and probably diluted by the dispersion in the individual offsets of the targets included. This implies that there are several discs in our sample with fluxes close to the 1σ noise of the individual observations.

3.3 General trends

In Fig. 7, we show our detections in the infrared colour–magnitude diagram used to divide the ODISEA sample into two (see Fig. 1). The detections are colour coded based on their observed 1.3 mm flux. The brightest millimetre sources occupy the upper envelope of the [*K*] versus [*K*]–[24] plane, which represent the brightest near-IR sources and/or the most embedded objects, which in turn tend to be embedded Class I sources and Class II discs around (relatively) more massive stars. Similarly, the fainter millimetre sources (< 3 mJy) tend to have fainter *K*-band fluxes and bluer [*K*]–[24] colours. Therefore, it is reasonable to suspect that most of the ODISEA targets that still remain to be observed (Sample B in Fig. 1) will be, on average, fainter at 1.3 mm. Also, the A_V = 25 mag extinction vector shown at the top left of the figure demonstrates that very high extinction can move sources across the IR SED classification (e.g. from Class III to Class II and from Class II to Flat Spectrum and Class I sources). This introduces some ambiguity in the physical interpretation of the SEDs Classes, which are purely based on the observed spectral slopes. For instance, while there is a strong correspondence between observationally defined Class I sources and theoretical Stage I objects (protostars surrounded by infalling envelopes; see Evans et al. 2009a), YSOs without associated envelopes might also be classified as Class I sources if they are found behind a dense molecular cloud.

We have searched the literature for multiplicity information and found that 25 of our targets have previously known companions within 5 arcsec. Our ALMA imaging survey has identified 4 additional binaries, for a total of 29 multiple systems among our 147 ALMA targets. We have also collected spectral types from the literature for 88 objects from our sample. The spectral types and the separations of the companions are listed in Table 1. In Fig. 8 (left-hand panel), we show the flux as a function of major axis for our sample. There is a general trend in the sense that brighter discs tend to be larger as already reported by Piétu et al. (2014) and Tripathi et al. (2017). However, we note that there is a very large dispersion of sizes for a given flux. For instance, discs with ∼50 mJy fluxes

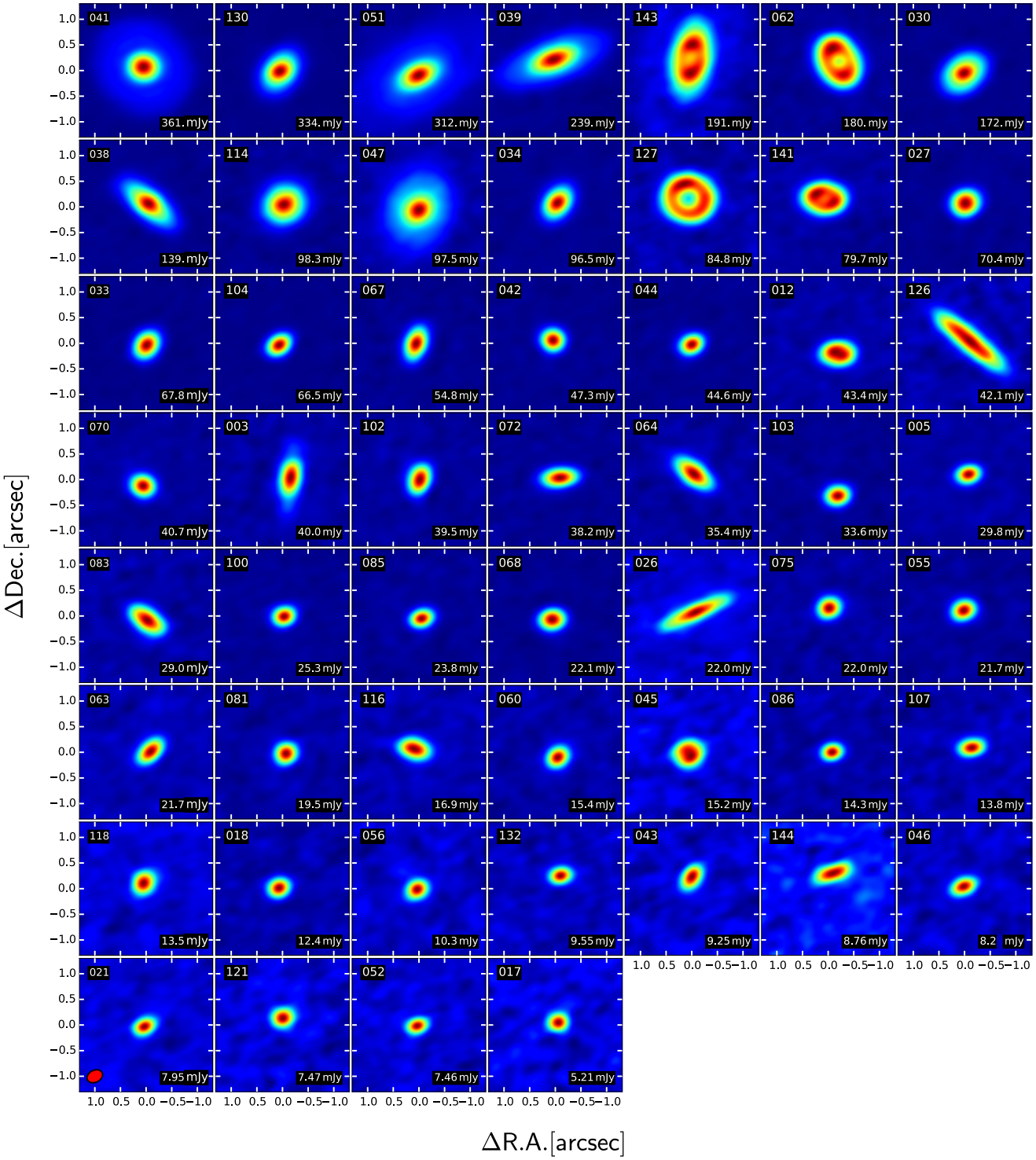

Figure 3. The 53 individual detections resolved by our 1.3 mm observations, ordered by decreasing integrated flux (provided at the bottom right of each panel).

have FWHM values that range from smaller than ∼0.1 arcsec to ∼1 arcsec, suggesting very different surface density profiles in the dust. Unresolved sources are typically faint ($F_{1.3,} \lesssim 10$ mJy). Discs with close companions (projected separations < 2.0 arcsec; shown with red symbols) tend to be small (FWHM < 0.2 arcsec or 28 au), with the exception of objects 022A and 141. Object 022A (see Fig. 5) has a relatively distant companion (1.78 arcsec or 250 au), while object 141 has recently been identified as a circumbinary disc using aperture masking imaging (Ruíz-Rodríguez et al. 2016). In this latter case, the separation of the companion is only 20 mas

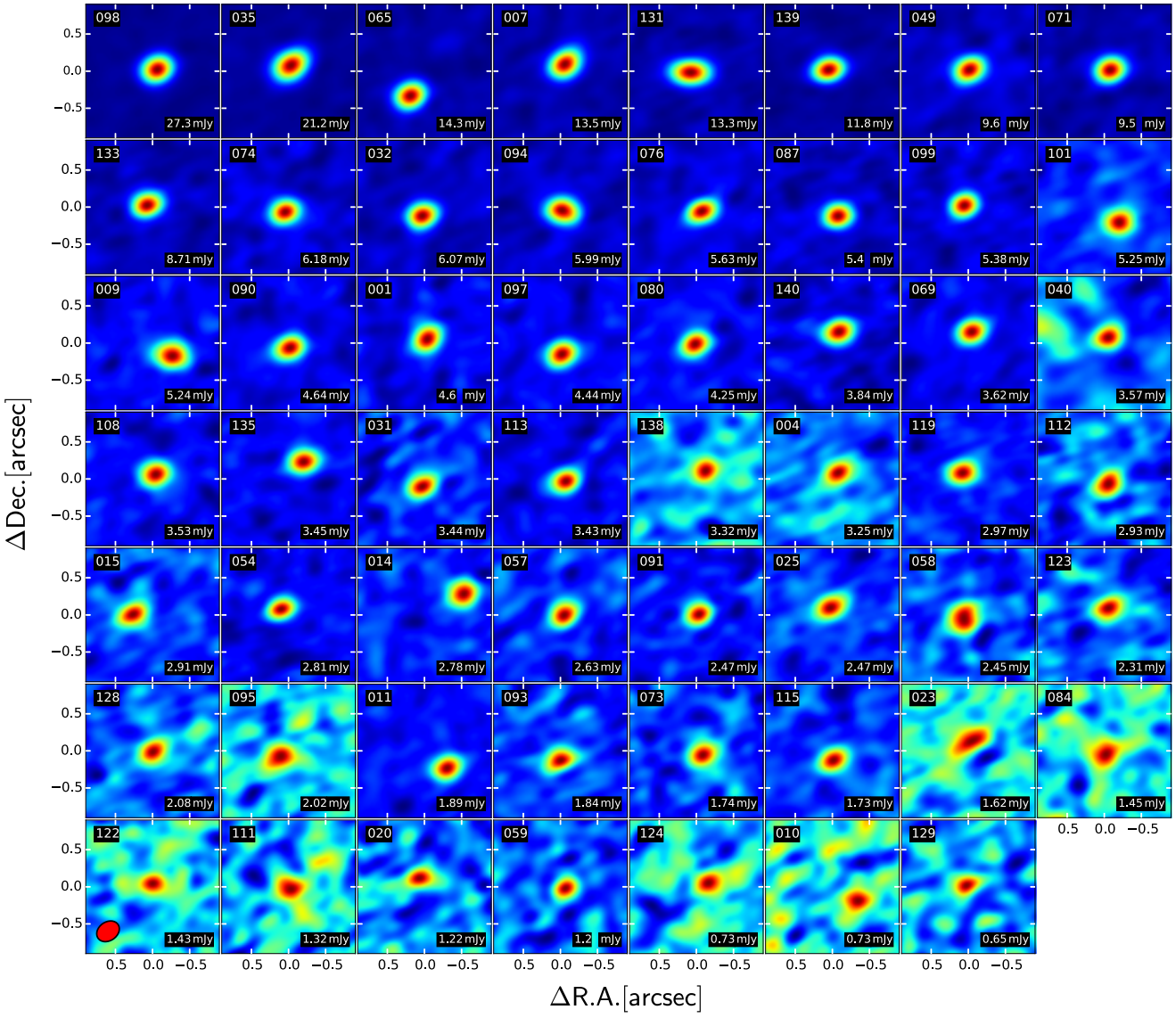

Figure 4. The 55 individual detections that remain unresolved in our 1.3 mm data, also ordered by decreasing integrated flux (provided at the bottom right of each panel).

(2.8 au). Stellar companions are known to decrease the incidence of circumstellar discs in young stars (Cieza et al. 2009; Kraus et al. 2012), especially in systems with separations of a few tens of au. Cox et al. (2017) recently demonstrated that discs in binary systems are also smaller and fainter than those around single stars, which is consistent with our results shown in Fig. 8. A detailed discussion of the effects of stellar companion on the properties of protoplanetary discs will be included in a future paper of this series (Zurlo et al. in preparation), which also presents a dedicated adaptive optics search for stellar binaries in Ophiuchus.

In Fig. 8 (right-hand panel), we also show the disc flux as a function of spectral type, which serves as a rough proxy for stellar mass. Disc properties as a function of stellar properties will be quantified and investigated in more detail in a follow-up paper from this series incorporating new optical and infrared spectroscopic observations (Ruíz-Rodríguez et al. in preparation). However, in our limited sample, we find that the fainter discs ($F_{1.3\mathrm{mm}} < 20$ mJy) are distributed across all spectral types, while the brighter discs ($F_{1.3\mathrm{mm}} > 100$ mJy) are clustered around spectral types in the K5 to M0 range in objects without known stellar companions.

In summary, from the initial analysis of the ODISEA sample we can report the following general trends: faint ($F_{1.3\mathrm{mm}} < 10$ mJy) and small (FWHM < 0.2 arcsec $\sim$28 au) discs are the most common type of discs in the Ophiuchus Molecular Cloud. They are seen across spectral types and SED Classes, and specially around stars in binary systems. Discs brighter than 50 and 100 mJy represent only $\sim$15 and $\sim$5 per cent of our sample of 147 objects, respectively. Given the trends seen in Fig. 7, which suggest that bright discs are already overrepresented in 'Sample A' with respect to 'Sample B', these very bright discs most likely account for even smaller fractions of the full population of *Spitzer*-detected discs. The brightest discs in our sample ($F_{1.3\mathrm{mm}} > 100$ mJy) are seen around (presumable) single stars with intermediate spectral types and seem to be missing at the edges of the spectral type distribution. There is a tendency for brighter discs to be larger, but the flux versus size relation shows a significant dispersion (a factor of $\sim$10).

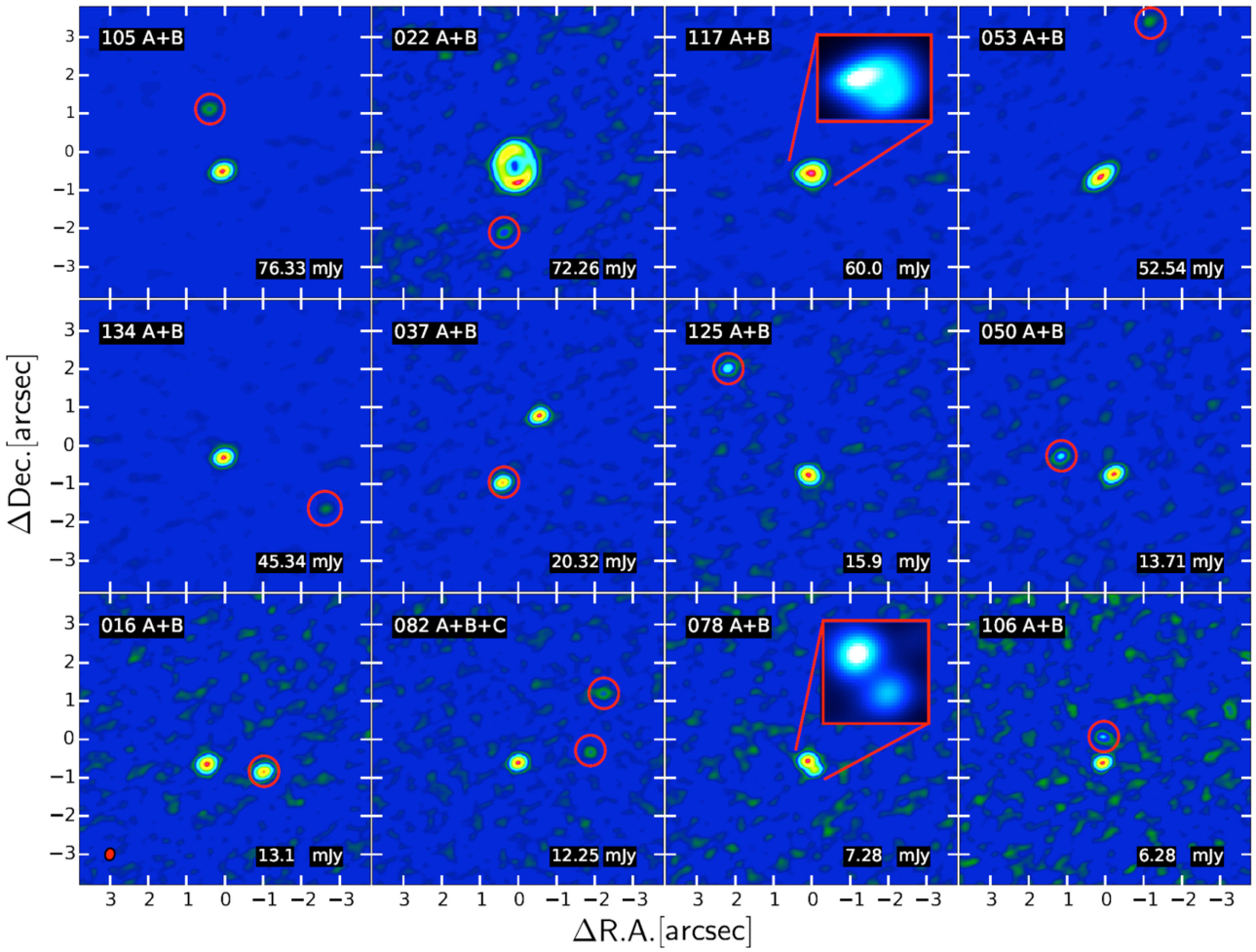

Figure 5. The 12 multiple systems in which discs are seen around each one of the individual components. The fluxes listed correspond to the primaries. Object 082 is a triple system, the rest are binaries. Object 117 is a known infrared binary that is only barely resolved by our ALMA observations. Companions are indicated with red circles or highlighted in insets of images with higher spatial resolution (i.e. uniform weights were applied in cleaning).

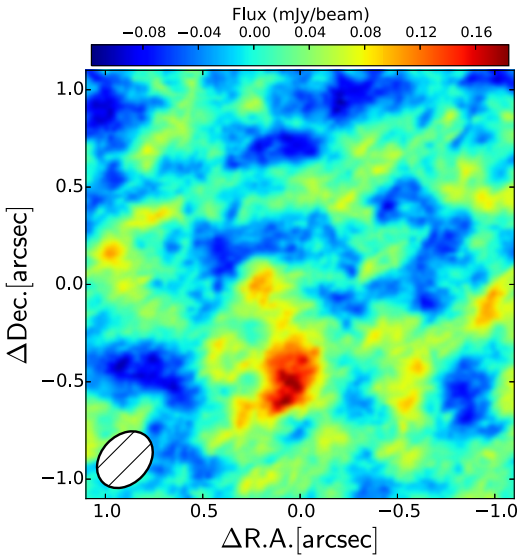

Figure 6. Stacking of the 27 non-detections showing a 0.16 mJy (4σ) detection with an offset of −0.5 arcsec in Dec., consistent with the mean Dec. offset seen in the detected discs.

3.4 Disc substructures

For the subset of ∼50 sources with fluxes $\gtrsim$15 mJy, we perform phase-only self-calibration and produced images with *uniform* weightings to increase the resolution from ∼0.2 arcsec to ∼0.15 arcsec and search for substructures in the discs. For this subsample, the average improvement in the peak signal-to-noise ratio (S/N) is 10 per cent, but the improvement can be as high as ∼50 per cent for the brightest sources. Below a flux level of 15 mJy, self-calibration does not significantly improve the S/N. A visual inspection of our images reveals a series of interesting substructures (see Fig. 9).

Objects 12, 22A, 62, 127, 141, and 143 show inner cavities of different sizes from barely resolved (object 12) to 1 arcsec in diameter (object 22). Object 41 shows two concentric gaps at 0.4 and 0.7 arcsec. Object 143 shows an external ring in addition to the inner cavity. Objects 62, 127, 141 (best known as EM* SR 24S, DoAr 44, and RX J1633.9-2442, respectively) had their cavities resolved by pre-ALMA observations (Andrews et al. 2011; Cieza et al. 2012b). The substructures in objects 12 and 143 (also known as IRAS 16201-2410 and WSB 82) were recently imaged by Cox et al. (2017). Object 41 (best known as Elias 2-24) was recently identified as a disc with a remarkable substructure almost simultaneously by three different groups (Cieza et al. 2017; Cox et al.

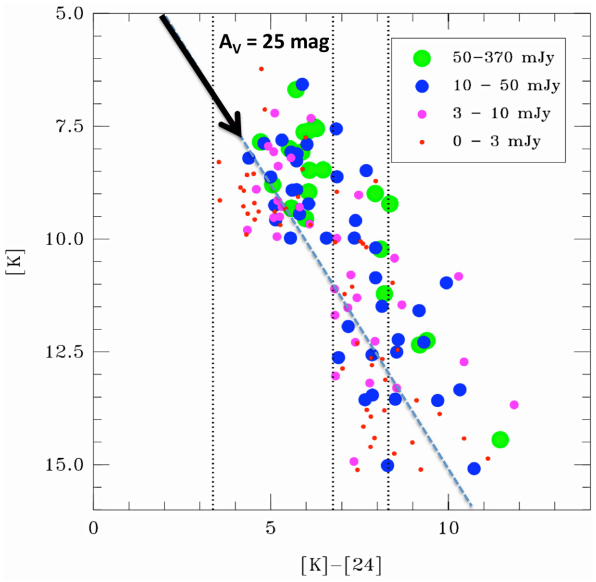

Figure 7. The *K*-band magnitude as a function of [*K*]–[24] colour for our Cycle-4 sample, with the sources colour coded by flux. ALMA non-detections are included on the lower bin (0–3 mJy). The black arrow represents an $A_V = 25$ mag extinction vector. As in Fig. 1, the vertical dotted lines are the approximate boundaries between Class III, Class II, Flat Spectrum, and Class I objects (left to right). Brighter sources tend to occupy the upper envelope of the [*K*] versus [*K*]–[24] plane (above the dashed diagonal line) and correspond to the brightest infrared sources and/or the most embedded objects.

2017; Dipierro et al. 2018). Object 51 (Elias 2-27) has spiral arms that were first identified by Pérez et al. (2016). Interestingly, object 22A (also known as ROXRA 3) has the disc with the largest cavity in our entire sample but was not previously known to host such a cavity.

We note that all 8 targets discussed above showing structures are brighter than ∼43 mJy and therefore are among the brightest 25 objects (∼17 per cent of the sample). This implies that ∼32 per cent (8/25) of the brightest objects show some type of substructures when observed at an ∼0.2 arcsec (∼28 au) resolution. Whether the fainter (usually smaller) targets show scaled-down versions of these substructures remains to be established by deeper and higher resolution observations.

To search for additional, more subtle substructures, we use the coordinates, position angles, and FWHM values of the major and minor axes listed in Table 3 to deproject the images and plot the deprojected radial profiles. Fig. 10 shows the images with uniform weightings and deprojected radial profiles for all targets with fluxes $\gtrsim$15 mJy and errors in PA < 90 deg that are consistent with smooth-disc structures. In Fig. 11, we show the images and profiles of four sources where the radial profiles have breaks in slope, which we interpret as possible hints for substructures (e.g. unresolved gaps). They are objects 30, 39, 47, and 114, which are best known as ROXR1 16, DoAr 25, *ISO*-Oph 54, and WSB 60, respectively. Using the same approach, DoAr 25 was already identified as a disc with a possible substructure by Cox et al. (2017). These four objects are among the brightest targets in the sample ($\gtrsim$100 mJy); therefore, if these substructures turn out to be real, it would imply that ∼50 per cent (11/21) of the sources brighter than $\gtrsim$50 mJy show some kind of substructure.

4 DISCUSSION

4.1 Disc dust masses and sizes

Since protoplanetary discs typically become optically thin at millimetre wavelengths outside the first few au, most dust particles in the disc contribute to the observed 1.3 mm fluxes; therefore, these values can be used to estimate the amount of dust present, as follows:

$$M_{\rm dust} = \frac{F_\nu d^2}{\kappa_\nu B_\nu(T_{\rm dust})}, \quad (2)$$

where F_ν is the flux, B_ν is the Plank function, and κ_ν is the dust opacity. Adopting the prescription for κ_ν at millimetre wavelengths from Beckwith et al. (1990),

$$\kappa_\nu = 0.1 \left(\frac{\nu}{10^{12}\,{\rm Hz}}\right)^\beta \ {\rm cm^2\ g^{-1}} \quad (3)$$

we obtain $\kappa_{1.3{\rm mm}} = 0.023$ cm^2 g^{-1} for $\beta = 1.0$. If we further adopt $d = 140$ pc based on recent VLBA and Gaia results (Ortiz-León et al. 2017; Canovas et al., in preparation) and $T_{\rm dust} = 20$ K, which is the median disc temperature in Taurus calculated by Andrews & Williams (2005), equation (2) then becomes

$$M_{\rm dust} = 0.58 \times \frac{F_{1.3{\rm mm}}}{\rm mJy} {\rm M_\oplus}. \quad (4)$$

The linear relation between flux and dust mass is supported by the fact that the Planck function is close to the Rayleigh–Jeans regime at millimetre wavelengths, $B_\nu \sim 2\nu^2\kappa T/c^2$, and the emission is only linearly (rather than exponentially) dependent on the dust temperature. While the average disc temperature might be lower than 20 K in the discs around brown dwarfs (van der Plas et al. 2016), as shown by Tazzari et al. (2017), the disc temperature does not depend strongly on stellar properties in the 0.1–2 $M_\odot$ stellar mass range. However, the optically thin assumption breaks down in the dense inner regions (Andrews & Williams 2007), and depending on the size of the disc and its surface density profile, the fraction of optically thick material might be significant even at 1.3 mm, resulting in *underestimated* disc masses. On the other hand, very compact discs around bright stars might have higher average temperatures than 20 K. If the temperatures are higher than the adopted 20 K value, disc masses would then be *overestimated*. Obtaining accurate masses for small and very dense discs might require high-resolution observations at longer wavelengths and detailed radiative transfer modelling. Fortunately, this is within the reach of ALMA capabilities, which can obtain 3.0 mm images at a 0.04 arcsec resolution (6 au at 140 pc). Disc masses from radiative transfer modelling of our sources will be presented by Pérez et al., (in preparation), but meanwhile, we estimate disc masses from equation (3), which are shown in Fig. 12 (left-hand panel). Using equation (3), we also find that the 0.16 mJy detection in the stacking analysis (Section 3.2) corresponds to an average dust mass of just 0.09 $M_\oplus$.

Besides the mass, the size is another fundamental property of a protoplanetary disc. Since protoplanetary discs do not have sharp edges, defining a size is not trivial. The large-scale radial structures of protoplanetary discs are often described by a characteristic radius and an exponential tapper in the outer disc (Hughes et al. 2008; Andrews et al. 2010; Cieza et al. 2018). Characteristic radii for all the spatially resolved sources will also be derived from radiative transfer modelling, but for now we simply show in Fig. 12 (right-hand panel) the distribution disc sizes derived in Section 3.1. Here we define the radius as FWHM/2 and show the values in au for the adopted distance of 140 pc. We emphasize that the disc sizes defined

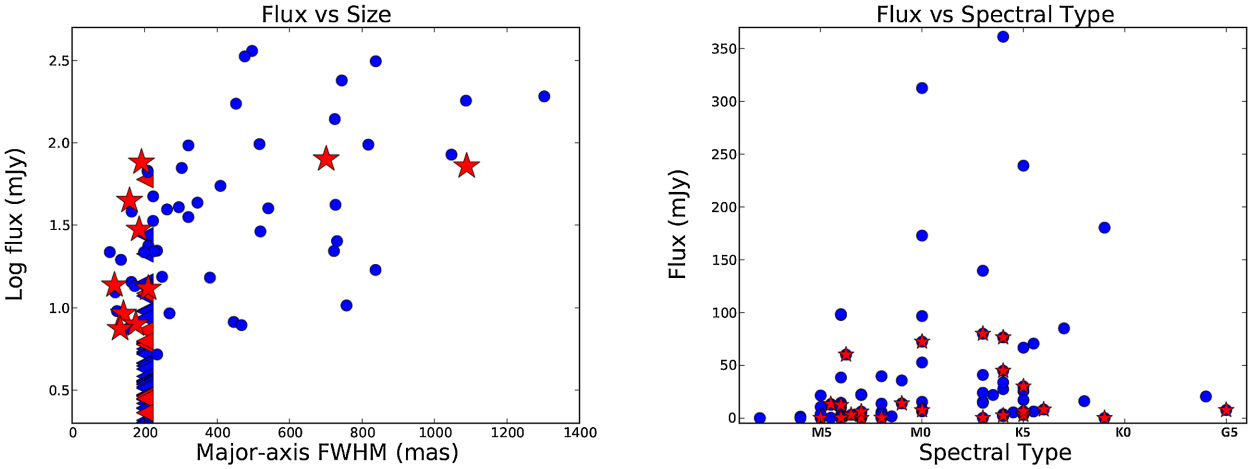

Figure 8. *Left-hand panel:* the 1.3 mm flux versus the FWHM of the detected discs. Members of multiple systems are shown in red. Unresolved sources (triangles) are shown with upper limits in disc sizes of 200 mas and are mostly clustered towards low fluxes ($\lesssim$10 mJy). Discs in multiple systems tend to be small, with a few exceptions (objects 022A and 141). While there is a large dispersion of sizes for a given flux, there is a general trend in the sense that brighter discs tend to be larger. *Right-hand panel:* the 1.3 mm flux of the disc versus the spectral type of the central object. Objects with close companions (projected separation < 2.0 arcsec) are indicated by red stars. Faint discs are seen around almost all types of stars, but the brightest discs ($F_{1.3\mathrm{mm}} > 100$ mJy) are mostly restricted to objects with types between M0 and K5 without known close companions.

this way are not equivalent to disc outer radii, which are typically very difficult to quantify. Depending on the signal to noise of the data, interferometers like ALMA are able to measure the size of a disc that is slightly smaller than the beam by deconvolving the beam from the signal. Therefore, relatively bright sources (e.g. S/N $\gtrsim$ 30) that are consistent with point sources are likely to be significantly smaller than the beam. For simplicity, we conservatively set the sizes of all the unresolved sources (55 single discs and 18 components of multiple systems) to an FWHM of 0.2 arcsec, corresponding to a radius of $\sim$14 au.

4.2 Comparison to other regions

As discussed in Section 1, ALMA has already surveyed many of the nearby star-forming regions and young clusters. This allows us to compare the distribution of dust masses seen in Ophiuchus to those in regions of different ages. In Fig. 13, we show the cumulative distribution of the dust masses seen in Ophiuchus calculated using the Kaplan–Meier estimator in the ASURV package (Lavalley, Isobe & Feigelson 1992) to include upper limits, as described by Ansdell et al. (2016). For a comparison, we perform the same analysis for objects in Lupus (Ansdell et al. 2016), Upper Scorpius (Barenfeld et al. 2016), Chamaeleon I (Pascucci et al. 2016), σ Ori (Ansdell et al. 2017), and IC 348 (Ruíz-Rodríguez et al. 2018). We also include the pre-ALMA study of Taurus (Andrews et al. 2013). The figure shows the ages for each region adopted in each one of the (sub)millimetre surveys, but note that these ages were not necessarily calculated in fully consistent ways.

We find that the dust mass distribution in our Ophiuchus sample (which is not yet complete) is very similar to those of other young regions (1–2 Myr) as Taurus and Lupus. However, significant evolution is seen towards older ages, as shown by recent studies (Ansdell et al. 2017; Ruíz-Rodríguez et al. 2018). Given the strong dependence of disc masses on stellar mass (Andrews et al. 2013), properly comparing the distribution of dust masses requires controlling the disc sample for stellar mass. For instance, the dependence on stellar mass explains why the discs in IC 348, a cluster dominated by very low mass stars, appear much fainter than the discs in Cham II, even though both clusters have a similar age. Their dust mass distributions are much more similar when accounting for the stellar mass dependence (Ruíz-Rodríguez et al. 2018). Spectral types can be used as a proxy for stellar mass but this becomes problematic when the range of stellar masses and ages increases because stars of a given stellar mass (specially solar mass and higher mass stars) do change spectral types during their pre-main-sequence evolution. Given these caveats, a more detailed comparison of the dust distribution seen in Ophiuchus to other regions will be presented by Ruíz-Rodríguez et al. (in preparation) using individually derived stellar masses and the full Ophiuchus sample. Based on the trends seen in Fig. 7 (lower disc masses towards lower K-band fluxes and bluer $[K]$–[24] colours), we anticipate that the dust mass distribution of Ophiuchus discs should move towards lower dust masses when Sample B is included.

4.3 Implications for planet formation: challenges and future directions

One of the main motivations of disc demographic studies like ODISEA is to inform planet formation models and constrain the planet formation potential of protoplanetary discs in nearby molecular clouds, which are very challenging tasks. While ALMA has unprecedented capabilities, it still provides limited information on the properties of protoplanetary discs and planet formation processes. The formation of rocky planets involves the growth of solid bodies over more than 12 orders of magnitude, from $\sim 10^{-6}$ to $> 10^{6}$ m scales (Lissauer 1993). However, ALMA is mostly sensitive to the emission of dust particles that are $\sim 10^{-3}$ m in size. Given the size distributions that are usually adopted for protoplanetary discs, with $n(a) \propto a^{-3.5}$ (Mathis, Rumpl & Nordsieck 1977) and a_{min} and a_{max} in the μm and mm regimes, respectively, most of the mass is contributed by the largest bodies in the distribution, and the total dust mass scales as $a_{\mathrm{max}}^{1/2}$. Therefore, (sub)millimetre fluxes constrain the mass of solids with sizes up to a few times the wavelength of the observations, but provide little information on the presence of larger bodies, beyond cm scales. This situation is complicated by the fact that radial drifting is a strong function of particle size

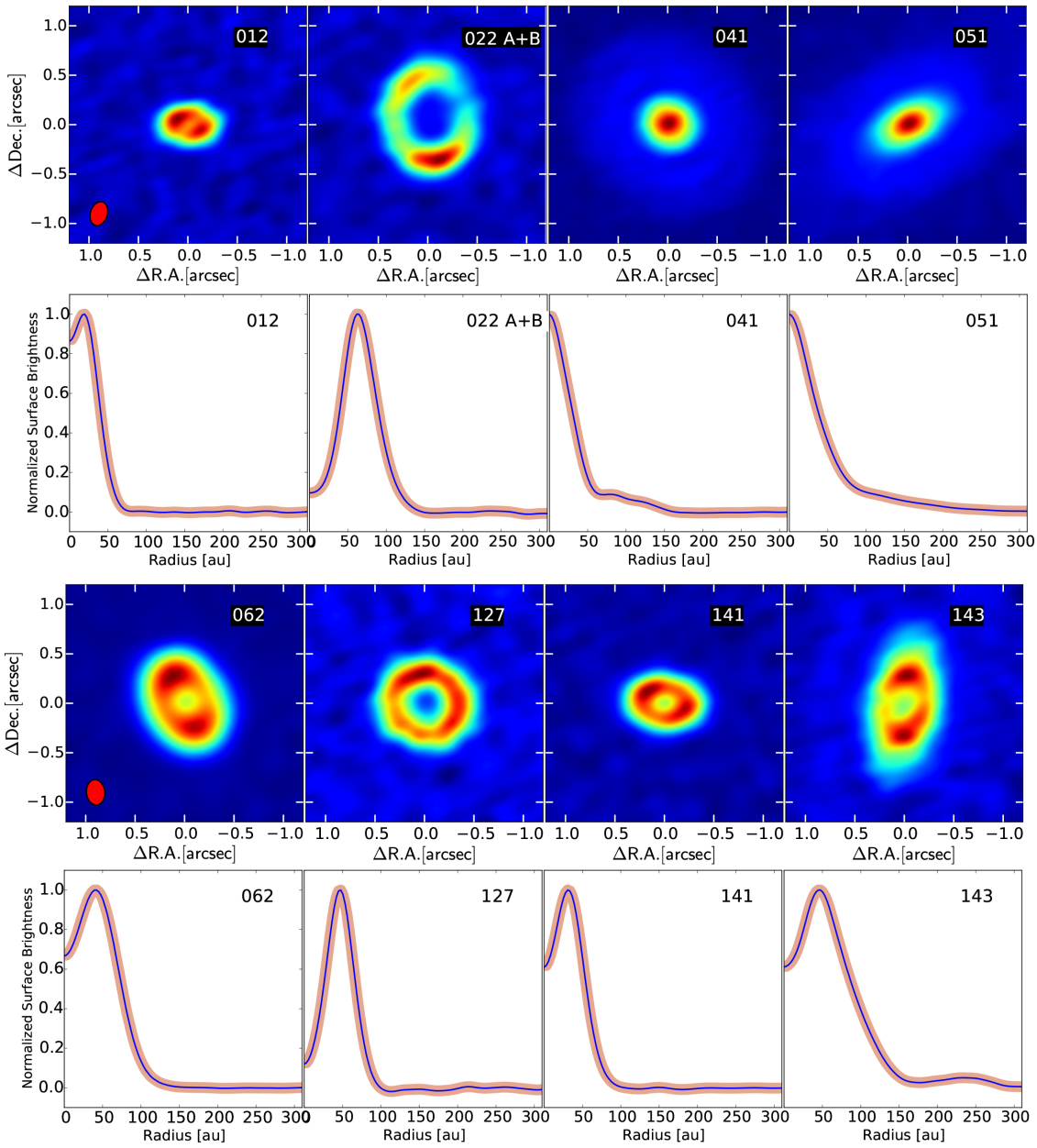

Figure 9. Images (top) and radial profiles (bottom) of the ODISEA objects with clear substructures: inner cavities, spirals, and/or narrow gaps. The red shade represents the 1σ error on the mean, given by the dispersion at a given radius divided by the square root of beams (i.e. the number of independent elements). The blue shade corresponds to the dispersion in azimuth at each radius.

(Birnstiel, Klahr & Ercolano 2012) and thus the grain-size distribution is a strong function of radius. Furthermore, snow lines produce radial discontinuities in the distribution of particle sizes (Banzatti et al. 2015). Similarly, gas giant planets are mostly made of H_2, which ALMA cannot directly observe. Instead, the gas content of protoplanetary discs is usually probed with other gas tracers like CO isotopologues, which are difficult to interpret (Miotello et al. 2017).

Very large objects might become detectable by ALMA, although indirectly, when they become massive enough to dynamically clear gaps in the disc. The minimum gap-opening mass depends on the viscosity and scale height of the disc (Duffell & MacFadyen 2013) but in any case requires fully formed planets, billions of times larger (in diameter) than the largest grains that are directly detectable by ALMA. Gaps consistent with being dynamically carved by fully formed planets have been imaged by ALMA in discs with estimated ages ranging from $\lesssim$1 Myr (HL Tau and Elias 2-24; ALMA Partnership et al. 2015; Cieza et al. 2017) to $\sim$10 Myr (TW Hydra; Andrews et al. 2016). However, the origin of these gaps still remains to be established and several alternative explanations have been proposed, including the snow lines of different species (Zhang, Blake & Bergin 2015; Okuzumi et al. 2016), magneto-hydrodynamic effects (Ruge et al. 2016; Flock et al. 2017), and viscous ring instabilities (Dullemond & Penzlin 2018).

Despite all the caveats discussed above, large ALMA surveys of protoplanetary discs still provide critical information on planet formation. The (sub)millimetre fluxes constrain the amount of raw solid material available for the formation of planets. In particu-

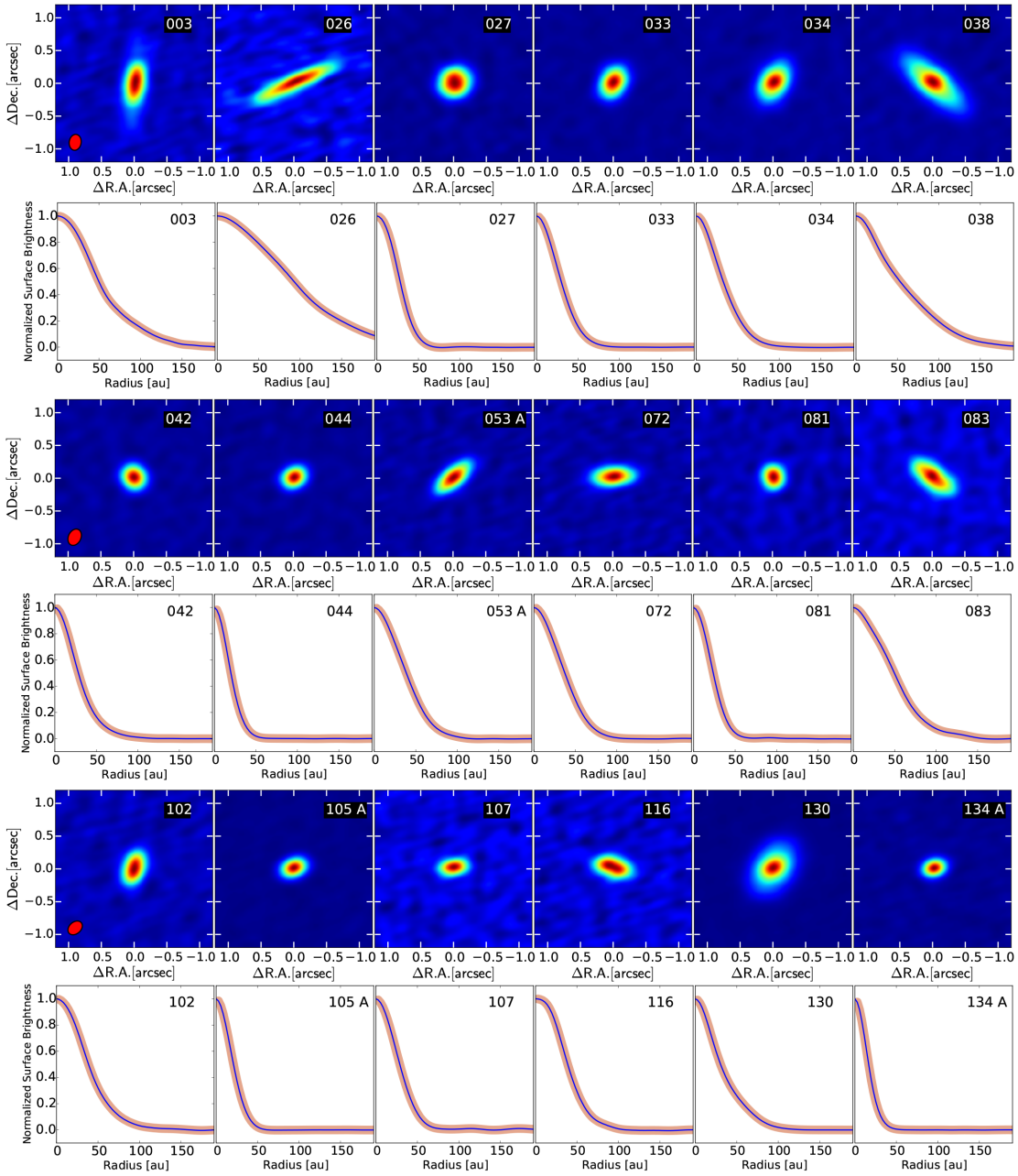

Figure 10. Images (top) and radial profiles (bottom) of the ODISEA objects consistent with continuous discs.

lar, the dust masses derived in Section 4.1 represent a lower limit to the amount of solids present in a given system. Also, relative dust masses are expected to be less uncertain than the absolute values, allowing the study of meaningful correlations between dust masses and stellar properties such as mass (Andrews et al. 2013), age (Ruíz-Rodríguez et al. 2018), multiplicity (Cox et al. 2017), and environment (Mann et al. 2014). As mentioned in Section 1, such correlations will be investigated in future ODISEA papers.

Based on the results from Section 4.1, we find that all detected sources (120 targets with $F_{1.3mm} \gtrsim 1$ mJy, or 82 per cent of the sample) have enough solids (in the form of dust) to form rocky planets ($M_{dust} \gtrsim 0.5$ $M_{\oplus}$). In contrast, only ∼50 targets (1/3 of the sample) have enough dust to form a critical-mass rocky core massive enough to start runaway gas accretion (∼10 $M_{\oplus}$; Lissauer 1993; Pollack et al. 1996) and trigger the formation of a gas giant. While these connections between disc properties and planet formation potential are just first-order approximations, they are in broad agreement with the relative incidence of extrasolar planets (Cassan et al. 2012; Howard 2013; Burke et al. 2015; Shvartzvald et al. 2016).

Other disc properties such as radius are less uncertain than absolute discs masses. The distribution of disc sizes shown in Fig. 12 (right-hand panel) suggests that planetary systems with compact architectures (e.g. most planets within 20 au) should be much more common than systems with planets in broad ($a > 20$ au) orbits, also in agreement with current constraints on extrasolar planets at these wide separations (Bowler 2016; Vigan et al. 2017). Similarly, if gaps and/or cavities like those discussed in Section 3.4 are in fact due to planets (e.g. Keppler et al. 2018), those features might be

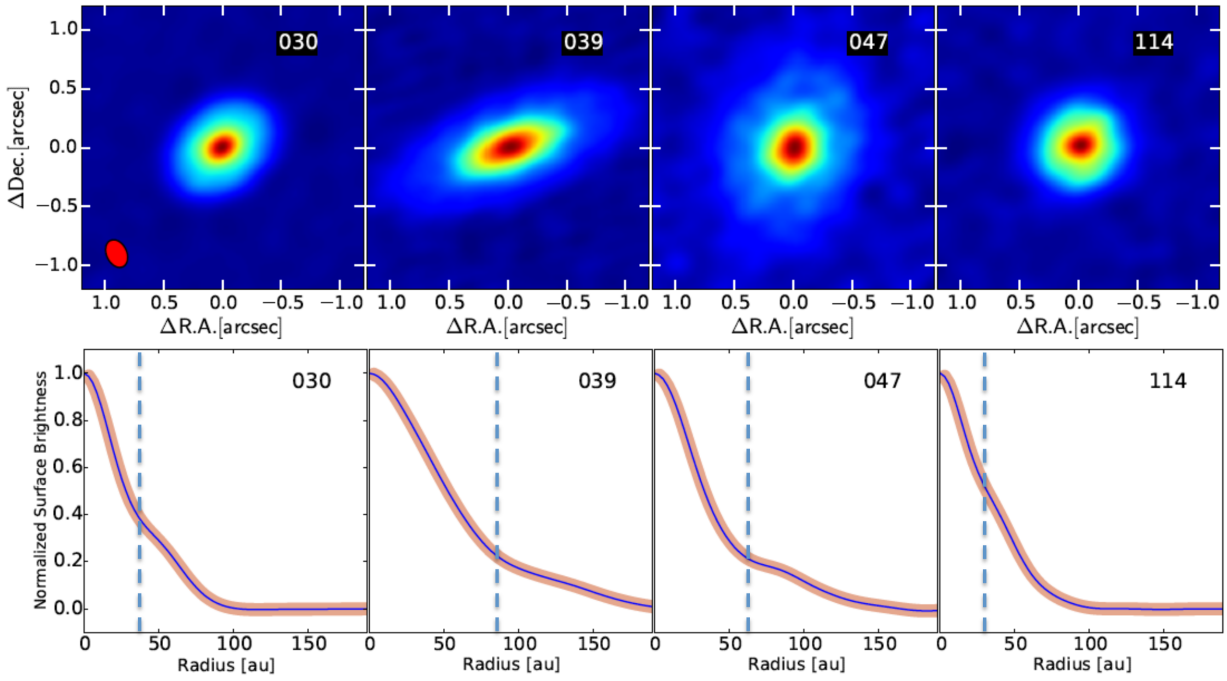

Figure 11. Images (top) and radial profiles (bottom) of the ODISEA objects with hints of substructures. The vertical lines show changes in slope indicating possible substructures.

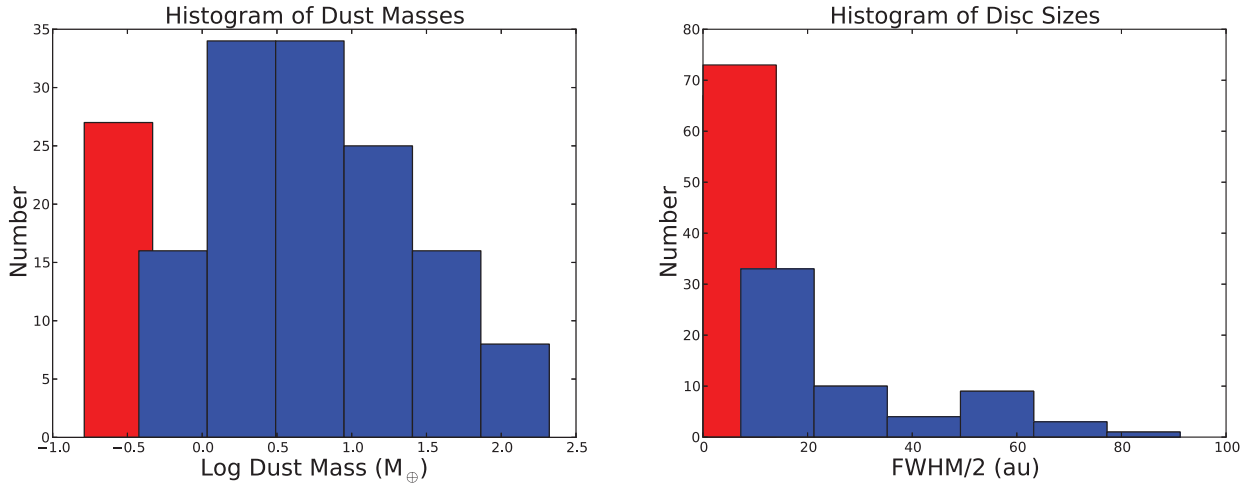

Figure 12. *Left-hand panel:* histogram of dust masses derived for our 133 detected discs. Mass upper limits (3σ) for the 27 non-detections are shown in red (first bar from the left). *Right-hand panel:* histogram of dust disc radii for 60 spatially resolved sources (7 of them correspond to binary systems), defined as 0.5 × FWHM of the major axis, and adopting a distance of 140 pc. A radius upper limit of 14 au has been assigned to 73 detected but unresolved discs (first bar from the left).

used to inform the incidence of different types of planets at different radii.

As disc studies are completed with ALMA and the searches for extrasolar planets continue to expand the parameter space (in terms of planet mass and semimajor axis), it will become easier to connect both fields. However, given the limitations of the disc observations mentioned above, which are unlikely to be solved in the foreseeable future, numerical modelling will remain the main way to investigate how the small dust particles that are observable by radio telescopes can grow into fully formed planets. In this context, disc demographic studies such as ODISEA can provide valuable input, in the form of basic disc parameters and their dependence on stellar properties, to planet population synthesis models (Alibert et al. 2005; Mordasini et al. 2009; Ronco, Guilera & de Elía 2017), which can then be used to connect disc populations to the populations of planets we see in the Galaxy.

5 SUMMARY

As part of the ODISEA project, we have observed 147 discs at a 0.2 arcsec (28 au) resolution in 1.3 mm continuum and CO isotopologues. In this first paper, we describe the scope of the survey, which aims to study the entire population of ∼300 protoplanetary discs identified by the 'Cores to Discs' *Spitzer* Legacy Project in

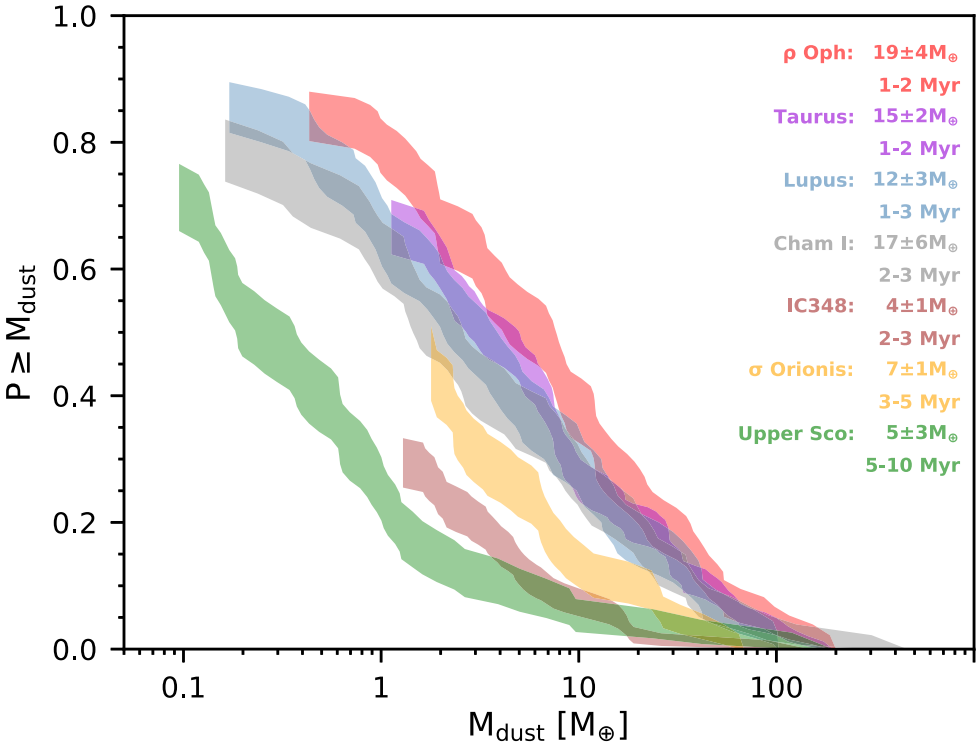

Figure 13. The cumulative dust mass distribution in our Ophiuchus sample compared to those of other young regions. The line widths indicate 1σ confidence intervals. Average dust masses and ages are listed for reference. Ophiuchus presents a disc mass distribution that is very similar to those seen in Taurus and Lupus, and more massive discs than older regions. However, the distributions shown are not corrected by sample selection biases or the dependence on stellar mass and thus should be interpreted with caution.

the Ophiuchus Molecular Cloud, and present the initial continuum data. Our main results are the following:

(1) We detect 120 of our 147 targets in 1.3 mm continuum, for an overall detection rate of 82 per cent. Among these detections, we find 11 binary systems and a triple system, for a total of 133 individual discs detected. Out of these 133 detected discs, 60 were spatially resolved and we measure fluxes, sizes, and position angles. The other 73 detected objects remain unresolved and we can only measure flux and set an upper limit to their size (approximately corresponding to the resolution of our observations).

(2) 27 of our targets remain undetected, with 4σ upper limits of $\sim$1.0 mJy, but a stacking of the non-detections shows a 4σ detection of 0.16 mJy, suggesting a typical dust mass of just $\sim$0.1 $M_\oplus$ for these objects.

(3) Among our sample, we find eight sources with clear sub-structures. Six of them have inner dust opacity cavities and two of them show narrow gaps/rings (one object, WSV 82, shows both an inner cavity and a gap/ring structure). Another object, Elias 2-27, shows two spiral arms. Four additional sources show hints of sub-structures based on their deprojected radial profiles. Most of these features are seen among the brightest sources in the sample. If they are all confirmed, it would imply that $\sim$50 per cent (11/21) of the sources brighter than $\sim$50 mJy show some type of substructure.

(4) We performed a preliminary comparison of the dust mass function in Ophiuchus to those of other regions. We find that the dust mass distribution in Ophiuchus is very similar to those of other young regions (1–2 Myr) as Taurus and Lupus. However, significant evolution is seen towards older ages, as already shown by previous results.

(5) A simple conversion between flux and dust mass (adopting standard assumptions for dust opacities and temperatures) indicates that all sources detected at 1.3 mm have enough solid mass to form one or more rocky planets. In contrast, only $\sim$50 discs ($\sim$1/3 of the sample) have enough mass in the form of dust to form the canonical 10 $M_\oplus$ core needed to trigger runaway gas accretion and the formation of gas giant planets. In this context, the main uncertainty is the total mass of solids already incorporated to large bodies (e.g. cm to km scales) that are not detectable by ALMA.

(6) The distribution in disc sizes in our sample is heavily weighted towards compact discs. Most discs have radii $<$ 15 au, while only 22 discs ($\sim$15 per cent of the targets) have radii $>$ 30 au. The discs that remain unresolved in our sample would benefit from higher resolution data at longer wavelengths to better constrain both their sizes and masses.

The detailed study of disc properties as a function of the mass and age of the host stars, the effects of (sub)stellar companions on disc properties, and the gas content in the discs based on the ^{12}CO, ^{13}CO, and C^{18}O observations will be presented in future papers of this series, along with radiative transfer modelling of resolved sources.

ACKNOWLEDGEMENTS

We thank the anonymous referee for his/her comments, which we believe have helped us to improve the manuscript significantly. This paper makes use of the following ALMA data: ADS/JAO.ALMA #2016.1.00545.S. ALMA is a partnership of ESO (representing its member states), NSF (USA), and NINS (Japan), together with NRC

(Canada), NSC and ASIAA (Taiwan), and KASI (Republic of Korea), in cooperation with the Republic of Chile. The Joint ALMA Observatory is operated by ESO, AUI/NRAO, and NAOJ. The National Radio Astronomy Observatory is a facility of the National Science Foundation operated under cooperative agreement by Associated Universities, Inc. LAC, SC, GHMB, AO, and AZ were supported by CONICYT-FONDECYT grant numbers 1171246, 1171624, 3170204, 1151512, and 3170657. DAR acknowledges support from NASA Exoplanets program grant NNX16AB43G. KPR acknowledges CONICYT PAI Concurso Nacional de Inserción en la Academia, Convocatoria 2016 Folio PAI79160052. LAC, SC, SP, and AZ acknowledge support from the Millennium Nucleus 'Protoplanetary Discs in ALMA Early Science', grant number RC130007. AB, JO, and MRS acknowledge support from the Millennium Nucleus for Planet Formation. GHMB also received funding from the European Research Council (ERC, grant agreement no. 757957). GvdP acknowledges funding from ANR of France under contract number ANR-16-CE31-0013 (planet-forming discs).

REFERENCES

Alibert Y., Mordasini C., Benz W., Winisdoerffer C., 2005, A&A, 434, 343
Allers K. N., Kessler-Silacci J. E., Cieza L. A., Jaffe D. T., 2006, ApJ, 644, 364
ALMA Partnership et al., 2015, ApJ, 808, L3
Andrews S. M., Williams J. P., 2005, ApJ, 631, 1134
Andrews S. M., Williams J. P., 2007, ApJ, 671, 1800
Andrews S. M., Wilner D. J., Hughes A. M., Qi C., Dullemond C. P., 2009, ApJ, 700, 1502
Andrews S. M., Wilner D. J., Hughes A. M., Qi C., Dullemond C. P., 2010, ApJ, 723, 1241
Andrews S. M. et al., 2011, APJ, 732, 42A
Andrews S. M., Rosenfeld K. A., Kraus A. L., Wilner D. J., 2013, ApJ, 771, 129
Andrews S. M. et al., 2016, ApJ, 820, L40
Ansdell M. et al., 2016, ApJ, 828, 46
Ansdell M., Williams J. P., Manara C. F. Miotello A., Facchini S., van der Marel N., Testi L., van Dishoeck E. F., 2017, AJ, 153, 240
Ansdell M. et al., 2018, ApJ, 859, 21
Banzatti A., Pinilla P., Ricci L., Pontoppidan K. M., Birnstiel T., Ciesla F. 2015, ApJ, 815, L15
Barenfeld S. A., Carpenter J. M., Ricci L., Isella A., 2016, ApJ, 827, 142
Bate M. R., 2018, MNRAS, 475, 5618
Beckwith S. V. W., Sargent A. I., Chini R. S., Guesten R., 1990, AJ, 99, 924
Birnstiel T., Klahr H., Ercolano B., 2012, A&A, 539, A148
Bowler B. P., 2016, PASP, 128, 102001
Burke C. J. et al., 2015, ApJ, 809, 8
Casassus S. et al., 2013, Nature, 493, 191,
Cassan A. et al., 2012, Nature, 481, 167
Chen H., Myers P. C., Ladd E. F., Wood D. O. S., 1995, ApJ, 445, 377
Cieza L. et al., 2007, ApJ, 667, 308
Cieza L. A. et al., 2009, ApJ, 696, L84
Cieza L. A. et al., 2010, ApJ, 712, 925
Cieza L. A., Schreiber M. R., Romero G. A., Williams J. P., Rebassa-Mansergas A., Merín B., 2012a, ApJ, 750, 157
Cieza L. A. et al., 2012b, ApJ, 752, 75
Cieza L. A. et al., 2013, ApJ, 762, 100
Cieza L. A. et al., 2016, Nature, 535, 258
Cieza L. A. et al., 2017, ApJ, 851, L23
Cox E. G. et al., 2017, ApJ, 851, 83
Currie T., Kenyon S. J., 2009, AJ, 138, 703
Cutri R. M. et al., 2003, The IRSA 2MASS All-Sky Point Source Catalog, NASA/IPAC Infrared Science Archive, tmc book
Dipierro G. et al., 2018, MNRAS, 475, 5296
Duffell P. C., MacFadyen A. I., 2013, ApJ, 769, 41
Dullemond C. P., Penzlin A. B. T., 2018, A&A, 609, A50
Dunham M. M., Crapsi A., Evans N. J., II Bourke T. L., Huard T. L., Myers P. C., Kauffmann J., 2008, ApJS, 179, 249
Erickson K. L., Wilking B. A., Meyer M. R., Robinson J. G., Stephenson L. N., 2011, AJ, 142, 140
Evans N. et al., 2009a, preprint (arXiv:0901.1691)
Evans N. J., II et al., 2009b, ApJS, 181, 321
Fernández-López M., Zapata L. A., Gabbasov R., 2017, ApJ, 845, 10
Flock M., Nelson R. P., Turner N. J., Bertrang G. H.-M., Carrasco-Gonzalez C., Henning T., Lyra W., Teague R., 2017, ApJ, 850, 131
Gaia Collaboration 2018, A&A, 616, A1
Gaidos E., Mann A. W., Kraus A. L., Ireland M., 2016, MNRAS, 457, 2877
Gáspár A., Rieke G. H., 2014, ApJ, 784, 33
Greene T. P., Wilking B. A., Andre P., Young E. T., Lada C. J., 1994, ApJ, 434, 614
Hardy A. et al., 2015, A&A, 583, A66
Howard A. W., 2013, Science, 340, 572
Hughes A. M., Wilner D. J., Qi C., Hogerheijde M. R., 2008, ApJ, 678, 1119
Keppler M. et al., 2018, A&A, 617, A44
Kohn S. A., Shkolnik E. L., Weinberger A. J., Carlberg J. K., Llama J., 2016, ApJ, 820, 2
Kraus A. L., Ireland M. J., Hillenbrand L. A., Martinache F., 2012, ApJ, 745, 19
Lavalley M., Isobe T., Feigelson E., 1992, in Worrall D. M., Biemesderfer C., Barnes J., eds, ASP Conf. Ser. Vol. 25, Astronomical Data Analysis Software and Systems I. Astron. Soc. Pac., San Francisco, p. 245
Lissauer J. J., 1993, ARA&A, 31, 129
Loinard L., Torres R. M., Mioduszewski A. J., Rodríguez L. F., 2008, ApJ, 675, L29
Luhman K. L., Rieke G. H., 1999, ApJ, 525, 440
Manara C. F., Testi L., Natta A., Alcalá J. M., 2015, A&A, 579, A66
Mann R. K. et al., 2014, ApJ, 784, 82
Mathis J. S., Rumpl W., Nordsieck K. H., 1977, ApJ, 217, 425
McClure M. K. et al., 2010, ApJS, 188, 75
McMullin J. P., Waters B., Schiebel D., Young W., Golap K., 2007, in Shaw R. A., Hill F., Bell D. J., eds, ASP Conf. Ser. Vol. 376,Astronomical Data Analysis Software and Systems XVI. Astron. Soc. Pac., San Francisco, p. 127
Miotello A. et al., 2017, A&A, 599, A113
Mordasini C., Alibert Y., Benz W., Naef D., 2009, A&A, 501, 1161
Okuzumi S., Momose M., Sirono S.-i., Kobayashi H., Tanaka H., 2016, ApJ, 821, 82
Ortiz-León G. N. et al., 2017, ApJ, 834, 141
Owen J. E., 2016, PASA, 33, e005
Pascucci I. et al., 2016, ApJ, 831, 125
Pérez L. M. et al., 2016, Science, 353, 1519
Piétu V., Guilloteau S., Di Folco E., Dutrey A., Boehler Y., 2014, A&A, 564, A95
Pollack J. B., Hubickyj O., Bodenheimer P. Lissauer J. J., Podolak M., Greenzweig Y., 1996, Icarus, 124, 62
Ratzka T., Köhler R., Leinert C., 2005, A&A, 437, 611
Rebollido I. et al., 2015, A&A, 581, A30
Ronco M. P., Guilera O. M., de Elía G. C., 2017, MNRAS, 471, 2753
Ruge J. P., Flock M., Wolf S., Dzyurkevich N., Fromang S., Henning T., Klahr H., Meheut H., 2016, A&A, 590, A17
Ruíz-Rodríguez D., Ireland M., Cieza L., Kraus A., 2016, MNRAS, 463, 3829
Ruíz-Rodríguez D. et al., 2018, MNRAS, 478, 3674
Shvartzvald Y. et al., 2016, MNRAS, 457, 4089
Tazzari M. et al., 2017, A&A, 606, A88
Tripathi A., Andrews S. M., Birnstiel T., Wilner D. J., 2017, ApJ, 845, 44
van der Marel N. et al., 2013, Science, 340, 1199
van der Plas G. et al., 2016, ApJ, 819, 102
Vigan A. et al., 2017, A&A, 603, A3
Wahhaj Z. et al., 2010, ApJ, 724, 835
Wilking B. A., Meyer M. R., Robinson J. G., Greene T. P., 2005, AJ, 130, 1733
Williams J. P., Cieza L. A., 2011, ARA&A, 49, 67

Zhang K., Blake G. A., Bergin E. A., 2015, ApJ, 806, L7

SUPPORTING INFORMATION

Supplementary data are available at *MNRAS* online.

Table 1. ODISEA Cycle-4 SAMPLE.
Table 2. Photometry from the *Spitzer* Cores to Discs Catalogue.
Table 3. Fluxes and sizes at 1.3 mm from Cycle-4.

Please note: Oxford University Press is not responsible for the content or functionality of any supporting materials supplied by the authors. Any queries (other than missing material) should be directed to the corresponding author for the article.

[1]*Facultad de Ingeniería y Ciencias, Núcleo de Astronomía, Universidad Diego Portales, Av. Ejercito 441. Santiago, Chile*
[2]*Millennium Nucleus 'Protoplanetary Discs in ALMA Early Science', Av. Ejercito 441, Santiago, Chile*
[3]*Chester F. Carlson Center for Imaging Science, Rochester Institute of Technology, Rochester, NY 14623-5603, USA*
[4]*Joint ALMA Observatory, Alonso de Cordova 3107, Vitacura 763-0355, Santiago, Chile*
[5]*National Radio Astronomy Observatory, 520 Edgemont Road, Charlottesville, Virginia, VA 22903-2475, USA*
[6]*Departamento de Astronomía, Universidad de Chile, Casilla 36-D Santiago, Chile*
[7]*European Space Astronomy Centre (ESA), Camino Bajo del Castillo s/n, E-28692 Villanueva de la Ca nada, Madrid, Spain*
[8]*Institute for Astronomy, University of Hawaii at Manoa, Honolulu, HI 96822, USA*
[9]*Department of Astronomy, University of California at Berkeley, Berkeley, CA 94720-3411, USA*
[10]*ETH Zurich, Institute for Particle Physics and Astrophysics, Wolfgang-Pauli-Strasse 27, CH-8093 Zurich, Switzerland*
[11]*Facultad de Ciencias, Instituto de Física y Astronomía, Universidad de Valparaíso, Av. Gran Bretaa 1111, 5030 Casilla, Valparaśo, Chile*
[12]*Millennium Nucleus for Planet Formation, Universidad de Valparaíso, Av. Gran Breta na 1111, Valparaíso, Chile*
[13]*Max Planck Institute for Astronomy, Königstuhl 17, D-69117 Heidelberg, Germany*
[14]*Instituto de Astrofísica de La Plata y Facultad de Ciencias Astronómicas y Geofísicas, UNLAP, Paseo del Bosque s/n, B1900FWA, La Plata, Argentina*
[15]*Centro de Astronomía (CITEVA), Universidad de Antofagasta, Av. Angamos 601, Antofagasta, Chile*
[16]*Massachusetts Institute of Technology, Kavli Institute for Astrophysics, Cambridge, 02139, MA, USA*
[17]*University Grenoble Alpes, CNRS, IPAG, F-38000 Grenoble, France*

This paper has been typeset from a TEX/LATEX file prepared by the author.